Journal of Medical Imaging

MedicalImaging.SPIEDigitalLibrary.org

Automated speckle tracking algorithm to aid on-axis imaging in echocardiography

Niti M. Dhutia
Graham D. Cole
Massoud Zolgharni
Charlotte H. Manisty
Keith Willson
Kim H. Parker
Alun D. Hughes
Darrel P. Francis

SPIE.

Automated speckle tracking algorithm to aid on-axis imaging in echocardiography

Niti M. Dhutia,[a,*] Graham D. Cole,[a] Massoud Zolgharni,[a] Charlotte H. Manisty,[a] Keith Willson,[a] Kim H. Parker,[b] Alun D. Hughes,[a] and Darrel P. Francis[a]
[a]National Heart and Lung Institute, Imperial College London, Hammersmith Hospital, W12 0NN, United Kingdom
[b]Imperial College of Science, Technology, and Medicine, Department of Bioengineering, London SW7 2AZ, United Kingdom

Abstract. Obtaining a "correct" view in echocardiography is a subjective process in which an operator attempts to obtain images conforming to consensus standard views. Real-time objective quantification of image alignment may assist less experienced operators, but no reliable index yet exists. We present a fully automated algorithm for detecting incorrect medial/lateral translation of an ultrasound probe by image analysis. The ability of the algorithm to distinguish optimal from sub-optimal four-chamber images was compared to that of specialists—the current "gold-standard." The orientation assessments produced by the automated algorithm correlated well with consensus visual assessments of the specialists ($r = 0.87$) and compared favourably with the correlation between individual specialists and the consensus, 0.82 ± 0.09. Each individual specialist's assessments were within the consensus of other specialists, $75 \pm 14\%$ of the time, and the algorithm's assessments were within the consensus of specialists 85% of the time. The mean discrepancy in probe translation values between individual specialists and their consensus was 0.97 ± 0.87 cm, and between the automated algorithm and specialists' consensus was 0.92 ± 0.70 cm. This technology could be incorporated into hardware to provide real-time guidance for image optimisation—a potentially valuable tool both for training and quality control. [DOI: 10.1117/1.JMI.1.3.037001]

Keywords: echocardiography; speckle tracking; ultrasound probe positioning; automated guidance.

Paper 14078R received Jun. 23, 2014; accepted for publication Oct. 31, 2014; published online Nov. 25, 2014.

1 Introduction

Transthoracic echocardiography, a noninvasive, portable and safe technique, is the day-to-day standard for assessing cardiac function and confirming or refuting the presence of valvular heart disease.[1] While the cost and portability of the equipment required has improved,[2] the availability of adequately trained operators is making it difficult to meet the elevating demand for cardiac ultrasound scans without compromising quality control.[3]

Clinical and research practice both require echocardiographic images to conform to consensus-agreed standards, to ensure reproducibility and correct interpretation.[4,5] Specialists in the field rely on experience to manipulate the ultrasound probe to an angle and position producing optimal images. Novices, however, frequently find it difficult to obtain "on-axis" images, because the relationship between probe movement and the resulting image orientation is not always intuitive. This may result in prolonged scanning time or inadequate images since real-time expert feedback is almost never available. An algorithm incorporated into the ultrasound hardware which could advise operators on how to manipulate the probe to optimize their images and confirm appropriate image orientation could be a useful tool in training and routine practice.

The primary purpose of this paper is to investigate the feasibility of using image processing techniques to identify off-axis images in echocardiography and deduce the probe adjustments required to obtain an on-axis image. This is the crucial prerequisite for our ultimate ambition to be able to deliver real-time analysis to obtain information on medial/lateral probe translation and feed this back to the operator during a scan. In such a future realization, the operator repeatedly makes adjustments to the probe until an adequate image is obtained and no further probe adjustments are required.

On-axis, standardized images are necessary in clinical practice, both to visualize all the structures of the heart, and to ensure standardized measurements. In the apical four-chamber view, seeing all four chambers and the mitral and tricuspid valves indicates that the image is on-axis and measurements of function can be compared against normal values, therefore, endocardial border definitions and orientation are important.[6] Off-axis probe positioning could result in suboptimal border definitions or foreshortening and suboptimal measurements.

The crucial challenge for a real-time guidance system is a suitable, reliable algorithm that is capable of full automation without human input. It is critical that such an algorithm is able to correctly identify appropriate image orientation at least as well as the method used in current clinical practice. However, currently there is no perfect "gold standard" even with guidelines, because even expert operators may interpret them slightly differently.

The only practical gold standard is, therefore, a consensus of several experts. It is necessary to quantify the extent of the inter-operator disagreement because no new method (however good) can agree with experts in general any better than they agree with each other.[7]

We observed that expert echocardiography operators use the pattern of longitudinal motion in addition to the explicit position

*Address all correspondence to: Niti M. Dhutia, E-mail: nitidhutia@gmail.com

0091-3286/2014/$25.00 © 2014 SPIE

of endocardial borders to determine whether images are correctly orientated. In this study, we set out to exploit this concept algorithmically by using speckle tracking, which tracks the random intensity patterns formed by speckles from frame to frame, in order to follow the motion of the myocardium.[8]

To our knowledge, there have been no tools developed to provide guidance to less-experienced operators on probe positioning to obtain appropriate images in echocardiography. Previous work has achieved automated image plane classification during three-dimensional (3-D) image acquisition,[9–11] using machine learning algorithms and Kalman tracking for automated segmentation. However, these were aimed at automatically classifying acquired standard two-dimensional (2-D) multiplanar reformatted planes from a 3-D volume. Snare et al.[12] use an extended Kalman filter framework to automatically distinguish between the standard 2-D two-chamber, four-chamber, and long-axis views.

Our algorithm proposes to analyze potentially imperfect, off-axis 2-D images and identify the probe adjustments for an operator to standardize their 2-D apical four-chamber image.

Weidenbach et al.[13,14] have developed a simulator to assist training in 2-D echocardiography. It consists of a surface model of the heart with registered echocardiographic volume data sets corresponding to each 2-D echocardiographic plane. The system uses a dummy ultrasound probe attached to a motion-tracking system to display the 2-D cutting plane selected at each probe position. This allows trainees to explore the 3-D heart model. This system uses reference datasets and is not capable of providing guidance for operators faced with scanning hearts of different shapes and sizes. Our strategy approaches the challenge of helping novice operators to acquire standardized images differently using global image properties, which will be comparatively resilient to variation between patients.

We present an algorithm that incorporates a combination of global image features and speckle tracking to identify correctly orientated apical four-chamber views. The aim of our algorithm is to automatically detect when 2-D apical four-chamber images are off-axis due to lateral or medial probe misalignment, which could potentially be used to provide feedback to an operator on how to maneuver the ultrasound probe to optimize the image.

2 Methods

Our automated algorithm, implemented in MATLAB (Mathworks Inc.), uses speckle tracking combined with global image properties to detect medial and lateral translation of an ultrasound probe for 2-D apical four-chamber images.

2.1 *Detection of Probe Translation*

2.1.1 *Speckle tracking and region detection*

A fully automated 2-D speckle tracking algorithm has been used, which implements a correlation-based method to track the motion of the myocardium from frame to frame across the whole image. Typical tissue motion in the septal and lateral walls during the systolic phase ranges from 7.5 to 10.3 cm/s, the early diastolic ranges from 10.9 to 17.3 cm/s, and the late diastolic ranges from 6.5 to 6.9 cm/s.[15,16] Our speckle tracking algorithm includes a series of noise-reduction stages using characteristics which include:

(i) Contrast—the underlying contrast of each kernel used for speckle tracking provides information contained within that kernel i.e., kernels containing myocardial tissue would have a high contrast and black regions within the chambers and bright white noisy regions would have a low contrast.
(ii) Neighbor consistency (across space)—the angle and magnitude of each speckle-tracked vector is compared with its four neighboring vectors. This gives an indication of the validity of that vector, since regional myocardial tissue should consistently move in the same direction at any given time point in the cardiac cycle.
(iii) Neighbor consistency (across time)—the velocity profile of each kernel across time should correlate well with the average velocity profile across time of the entire image. Noisy regions within the image would not follow the same pattern across time.
(iv) Validity of block matching—the best matched block for each kernel is used to determine the direction and magnitude of movement of that kernel. If all the blocks have a high correlation, the highest of these will be chosen as the best-matched block. This may be unreliable, however, therefore only blocks with a significantly higher correlation compared to other blocks based on statistical skewness are considered as reliable vectors. Additionally, the profile along the x and y directions of the block of correlations is also used as an indication of validity of the block matching result. This is because as we move further away from the best-matched block in any direction, the correlation should consistently decrease, giving a parabolic shape.

Each vector is assigned a normalized weighting representing its reliability based on these characteristics.

The average vertical component of these velocity vectors can be calculated for each frame, giving an estimation of the start and duration of systole and diastole during the cardiac cycle. Throughout the manuscript, we use the term "vertical" to refer to the component of the velocity along the y-axis which is vertical in the image as conventionally displayed to the operator, with the probe notionally positioned at the top of the screen. Except for points at the centerline, this component is not the same as the axial component toward the probe.

We then use the unique antiphase behaviour of the mitral and tricuspid valves during diastole to identify them. When the myocardial muscle relaxes, the muscle moves "away" from the apex, but the valves, open for ventricular filling, are moving "toward" the apex. The region of velocity vectors pointing apically during the diastolic frames of the video loop is identified as the valve region and deleted from the image for further analysis.

The next step is to locate the fastest-moving regions in the image after the mitral and tricuspid valve regions are deleted, which should be the interventricular septum and the left and right ventricular free walls. The vector direction of their movement can then be used to classify whether an image is on or off-axis. In essence, an on-axis image will have its predominant motion axially aligned toward/away from the probe.

In order to locate these walls, an automated region-growing algorithm based on Hojjatolesalami and Kittler's[17] approach is applied to the speckle-tracked vectors based on their reliability weighting and velocity. First, the vectors with a normalized reliability weighting less than 0.5 are eliminated. We then compute the normalized reliability-weighted, speckle-tracked velocities for the remaining vectors from the previous stage: these are the values used for the region-growing stage.

For region-growing, a seed pixel is automatically selected based on the highest reliability-weighted velocity vector. The region is grown around this seed pixel by adding neighboring pixels based on their weighted velocities until the difference between the neighboring pixels and the mean weighted velocity of the region exceeds 25% of the value of the seed pixel. This region growing process is repeated to find three regions.

Figure 1 shows an example of a grayscale apical four-chamber image superimposed with the three regions found using the region growing algorithm. Mean regional velocities are calculated for each region in each frame. For images not containing a clear view of the four chambers, three regions may not be detectable by the algorithm, in which case any two regions found, or even a single region in some cases, may be used to calculate the mean velocity.

The vertical components of the mean regional velocities from each of the three regions (Fig. 1) allow us to identify the systolic and diastolic phases of the cardiac cycle. For the timing assessment, the vertical component of velocity is used. For this stage, this is an acceptable simplification because the motion of the myocardium is primarily in the vertical direction.

2.1.2 *Using intercept to detect probe translation*

In apical four-chamber images, medial and lateral translation of the probe affects the position of the apex of the heart in relation to the center of the image. The main difficulty faced by novices in echocardiography is the non-intuitive relationship between probe motion and the resulting image orientation. One of the properties of the overall mean velocity vector calculated from the previous stage is that it points toward the apex of the heart during systole since the ventricles contract longitudinally toward the apex. Therefore, by locating the position of the apex using this mean vector, we can identify whether the apex is horizontally centered in the image. Because of the curvature of the chest and the position of the heart within it, translation of the probe to the left/right away from the apex results in a combination of rotation ad translation of the resulting image, with the apex displaced to the right/left of the center of the imaging plane. Correcting this translation brings the apex to the central location and corrects the rotation of the image.

Using the cardiac timing curve, the algorithm can automatically determine the frames that consist of the systolic phase of the cardiac cycle and average the overall velocity vectors from only these frames to obtain an average orientation vector for the image during systolic contraction. We then extend the orientation vector upward within the image and find where it intercepts the top edge of the image and calculate any displacement to the left or right, relative to the center of the image. The displacement is measured in pixels and then converted to centimeters using the known scale. Figure 2 illustrates how the intercept can be used to detect the direction and amount of translation for an on-axis apical four-chamber image and two apical four-chamber images with medial and lateral probe translation.

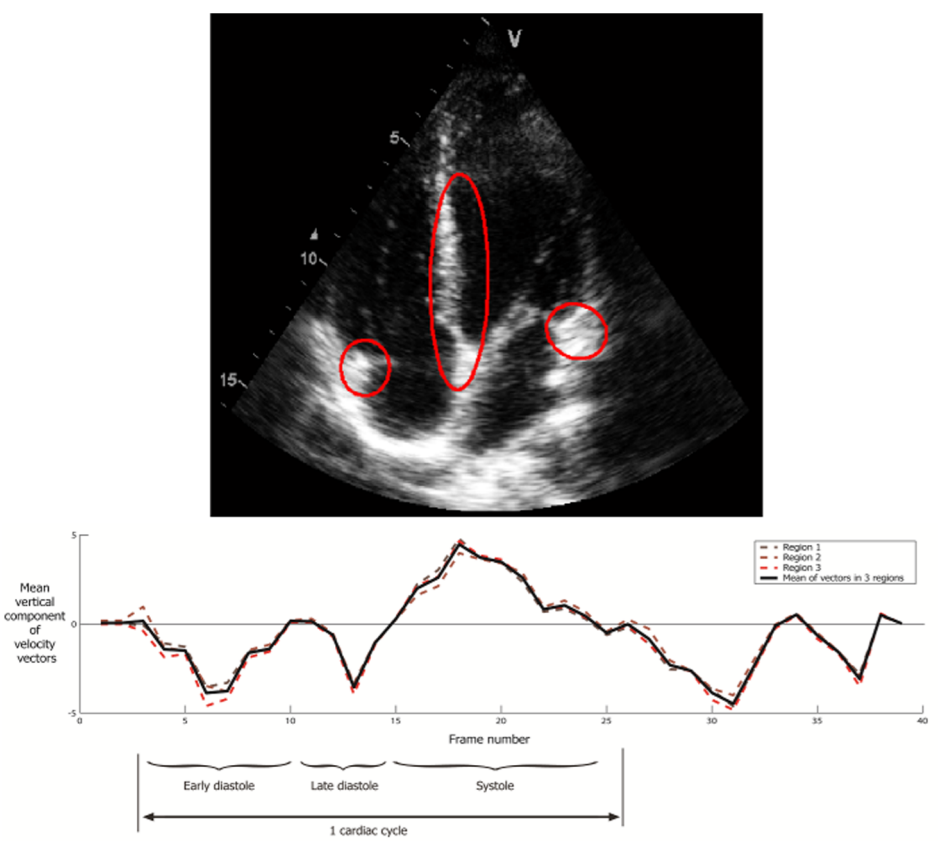

Fig. 1 Top: 2-D grayscale apical four-chamber view superimposed with the three high velocity regions (red ellipses)—the septum and left and right free walls, automatically identified by the region growing algorithm. Bottom: vertical component of the velocity vectors from each region, found by the automated region growing algorithm, showing the different phases of the cardiac cycle. The upward peak (positive velocities) represents the systolic phase of the cardiac cycle, and the two downward peaks (negative velocities) represent the early and late diastolic phases.

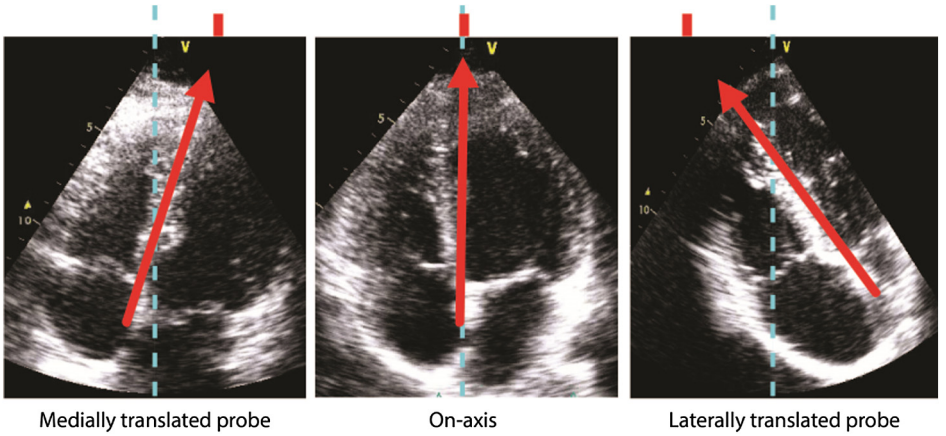

Fig. 2 2-D grayscale apical four-chamber images showing how the intercept of the overall mean velocity vector (red arrow) with the top of the image, relative to the center (dashed blue line), can be used to distinguish between an on-axis (middle) and medially (left) or laterally (right) translated probe positions.

2.1.3 *Processing time*

All the algorithms described above have been implemented in Matlab and require 2 to 3 s on average to analyze each pair of frames, which is not fast enough for real-time analysis. All the analysis in this study was carried out offline as a proof-of-concept. However, the same algorithms could be executed in real-time using programming languages with lower time overheads and by harnessing multicore computing systems for parallel processing.[18] Such steps should be able to deliver a 100-fold increase in speed and hence real-time capabilities.

2.2 *Algorithm Testing*

2.2.1 *Images*

The automated algorithm was tested on a set of 75 anonymized apical four-chamber video loops, acquired from 15 healthy normal subjects, with no significant myocardial abnormality, using a GE Vivid i machine. The research protocol was approved by the local ethics committee, and each subject gave prior written informed consent. Each subject's images consisted of five separate 2-D grayscale apical four-chamber AVI video loops of an average of three cardiac cycles taken in each subject. The five video loops included both optimal and suboptimal probe positions, and images were of variable quality. The resolutions of the videos were 640×480 pixels and the average scale was 0.04 cm/pixel.

The acquisition frame rates ranged from ~50 to 70 Hz, however, due to compression the AVI file frame rates dropped to ~30 to 50 Hz. This lies within the range of "optimum" frame rates for speckle tracking based on previous studies.[19] Lower frame rates could result in the speckle pattern changing significantly between frames, and since speckle tracking relies on searching for a pattern in consecutive frames which is similar to and in close proximity to the reference frame, this would result in poor tracking. Higher frame rates do not necessarily improve the tracking and are sometimes achieved at the cost of lower spatial resolution, which means a poorly defined speckle pattern and, therefore, lower tracking quality.

2.2.2 *Data analysis*

All 75 video loops from the 15 echocardiographic studies were analyzed by six experienced echocardiography specialists who were asked to assess whether the images were correctly orientated or misaligned. For the images they classified as incorrectly orientated, they were asked to additionally indicate the direction and extent of probe translation on a centimeter scale. Out of the 75 video loops, 25 randomly selected video loops were unknowingly reassessed by the operator in the same session in order to determine the intra-operator variability.

Each specialist's translation advice was recorded on a centimeter scale—lateral probe translation was represented by negative displacements, medial probe translation by positive displacements, and on-axis images by zero displacement. Figure 3 shows a representative set of 5 images out of the 75 analyzed altogether to illustrate the scale used by the specialists when analyzing the images.

2.2.3 *Use of consensus opinion as a gold standard for comparison*

Because there is no widely-accepted, independent, quantitative method for assessment of the adequacy of image orientation, the average of the translation values of the six specialists was used as the consensus, and the performance of the individual specialists and the algorithm were assessed in reference to this specialists' consensus.

The discrepancy between the algorithm and specialists' consensus was calculated as the distance between the algorithm's translation values and the average of specialists' translation values. The discrepancy between individual specialists and the specialists' consensus was quantified as the distance between their translation values.

2.3 *Statistical Analysis*

Pearson product-moment correlation and Bland–Altman[20] analysis were used to measure the linear correlation and the agreement between the automated algorithm, individual specialists and the specialists' consensus. The inter- and intra-operator agreement of specialists is also calculated using these methods. The bias is expressed as the mean difference between the algorithm and specialists' translation values and assesses the tendency for either to over- or underestimate translation. The limits of agreement are calculated as two standard deviations of the difference between the algorithm and specialists' translation values and provide the interval within which 95% of the

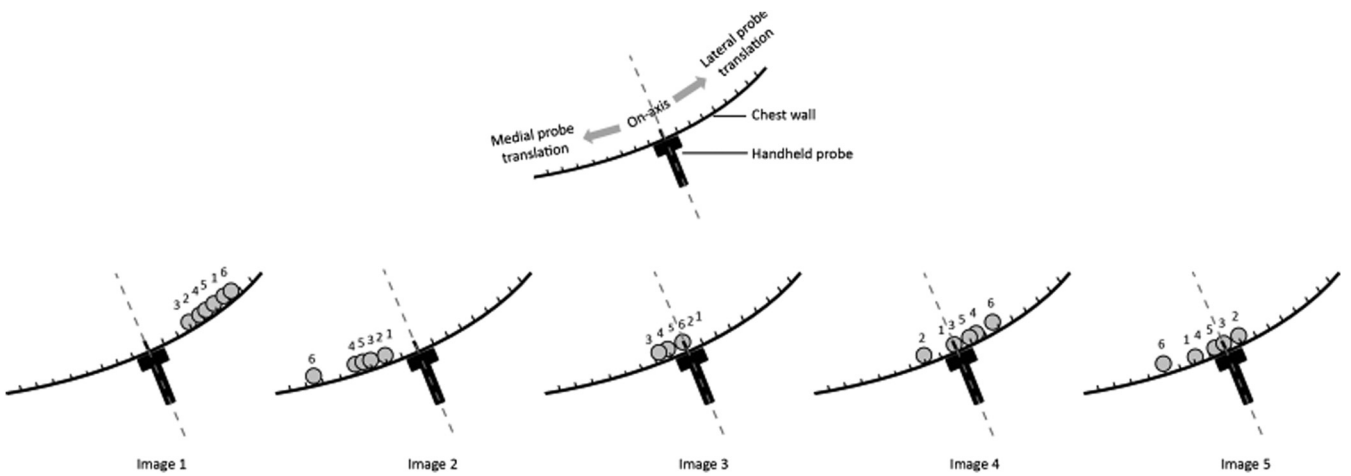

Fig. 3 Each specialist was asked to indicate the direction and amount of probe translation for each image, by marking its position on a cm representative scale, relative to an on-axis probe positioned correctly on the chest wall, as shown in this figure. The circles labelled 1 to 6 indicate probe translation advice from each of the specialists for 5 representative images out of the 75 images analyzed altogether.

differences between the two methods are expected to lie. All values are presented as mean ± standard deviation, and the threshold of statistical significance was set at the 5% level for all analyses.

3 Results

The specialists and the automated algorithm were able to assess all 75 video loops in the study.

3.1 *Individual Specialists*

Table 1 shows correlation coefficients for the agreement between individual specialists and their agreement with themselves on representation. The average interoperator correlation coefficient was 0.72 ± 0.12 and intra-operator correlation was 0.86 ± 0.13. The interoperator variability in translation values was 1.51 ± 0.85 cm; within operator, it was 0.80 ± 0.83 cm.

The limits of agreement between the individual specialists and the rest of the specialists are shown in Table 2. Bland–Altman analysis showed no statistically significant bias between any pair of specialists.

3.2 *Quantitative Orientation Agreement between Automated Algorithm and Individual Specialists*

The algorithm performed at least as well as any individual specialist, having an average correlation coefficient of 0.77 ± 0.04 with individual specialists (Table 1), which is noninferior to the correlation coefficient between pairs of specialists, 0.72 ± 0.12. The average discrepancy in translation values between the algorithm and individual specialists was 1.36 ± 1.10 cm, which is again noninferior to the discrepancy between pairs of specialists (interobserver variability), 1.51 ± 0.85 cm.

Table 1 Correlation coefficients showing inter-operator agreement, intra-operator agreement (shown in bold values) agreement between the algorithm and individual specialists and agreement between specialists, the algorithm and the consensus of the specialists. The last row shows the agreement between individual specialists and the consensus of specialists (excluding, in each column, that column's individual specialist, to avoid bias); in the final column, the automated algorithm is compared to the consensus of all the specialists.

Specialist	1	2	3	4	5	6	Automated algorithm
1	**0.96**	—	—	—	—	—	0.78
2	0.78	**0.76**	—	—	—	—	0.79
3	0.67	0.78	**0.63**	—	—	—	0.76
4	0.87	0.71	0.66	**0.90**	—	—	0.80
5	0.84	0.71	0.52	0.76	**0.96**	—	0.76
6	0.79	0.61	0.44	0.80	0.83	**0.94**	0.70
Specialist consensus	0.95	0.86	0.75	0.92	0.89	0.86	0.87
Specialist consensus excluding the individual specialist	0.92	0.80	0.67	0.88	0.85	0.80	0.87

Table 2 Limits of agreement from Bland–Altman analysis between pairs of specialists, between the automated algorithm and individual specialists and between the algorithm, individual specialists and the consensus of the specialists. Values are shown in centimeters.

	Specialist						
$n = 75$	1	2	3	4	5	6	Automated algorithm
1	—	—	—	—	—	—	0.48 ± 3.21
2	0.05 ± 3.21	—	—	—	—	—	0.43 ± 2.79
3	0.20 ± 3.83	0.14 ± 3.21	—	—	—	—	0.29 ± 2.94
4	0.07 ± 2.90	0.20 ± 3.83	-0.12 ± 4.43	—	—	—	0.41 ± 3.54
5	0.33 ± 2.82	0.07 ± 2.90	0.13 ± 3.87	0.25 ± 3.84	—	—	0.16 ± 2.94
6	1.15 ± 3.89	0.33 ± 2.82	0.95 ± 5.86	1.08 ± 3.90	0.82 ± 3.91	—	-0.67 ± 4.61
Consensus of specialists	0.36 ± 2.07	0.30 ± 2.80	0.12 ± 3.55	0.27 ± 2.96	-0.03 ± 2.42	-1.02 ± 4.03	0.18 ± 2.25

Bland–Altman analysis showed no statistically significant bias between the automated algorithm and any individual specialist. The limits of agreement between them are shown in Table 2.

3.3 *Quantitative Orientation Agreement Between Automated Algorithm and Specialists' Consensus Compared to the Agreement between Individual Specialists and Specialists' Consensus*

Figure 4 shows the relative translation values from individual experts and the automated algorithm for all 75 images. Each individual expert's translation values were within the specialists' consensus (the gold standard of comparison used in this study), $75 \pm 14\%$ of the time, whereas the algorithm's translation values were within the consensus of the specialists 85% of the time.

There was a fairly strong correlation between the automated algorithm and the specialists' consensus, $r = 0.87$, $p < 0.001$, with no statistically significant difference between the automated algorithm's and individual specialists' translation advice. The variability between specialists is indicated by the error bars in Fig. 5.

The agreement between the automated algorithm and the specialists' consensus (0.87) was also comparable to the agreement of individual specialists with the consensus of the rest of the specialists excluding their own (0.82 ± 0.09), as shown in Table 1. Therefore, the automated algorithm agrees with the specialists' consensus at least as well as individual specialists agree with the consensus.

The discrepancy in translation values between the algorithm and specialists' consensus (0.92 ± 0.70 cm) was no higher than that of individual specialists from the consensus (0.97 ± 0.87 cm).

Figure 6 shows the Bland–Altman plot of the automated algorithm against the specialists' consensus.

4 Discussion

Currently, obtaining a correctly orientated image is a skill developed by experienced echocardiographers. This requires training and "hands-on" experience, initially supervised by experienced operators whose own productivity is sacrificed to provide this early guidance. An automated method to guide the correct acquisition of a four-chamber image is likely to assist less experienced operators while promoting a robust governance framework. Our algorithm can predict the amount of translation of the probe required, which could, if implemented using faster hardware in the future, be fed back to an operator to help the acquisition of standardized images to ensure reproducibility and correct interpretation.

This study shows proof-of-concept of a fully automated algorithm to identify medial and lateral translation of a hand-held ultrasound probe for four-chamber echocardiography images. The automated algorithm was noninferior to expert echocardiography specialists on all measures.

4.1 *How Does the Automated Algorithm Compared with Specialists?*

The results show that algorithms such as this can be used to detect medial and lateral probe translation for four-chamber echocardiography images as reliably as trained echo specialists inspecting the image. The algorithm consistently identified the direction and amount of translation within the range of those provided by individual specialists and correlated well with the specialists' consensus.

The discrepancy between the automated algorithm and the specialists' consensus was no higher than the inter- and intra-operator variability, therefore, the algorithm does not increase the degree of error that exists within the current 'gold standard'.

Algorithm development appears now to have reached a stage where it can perform as well as human experts, therefore, future development may need new ways of testing for improvement.

4.2 *How Many Degrees of Freedom might an Operator Guidance System Need?*

A hand-held ultrasound probe has, in practice, 5 degrees of freedom. Three of these are angular—rotation about its own axis, medial/lateral tilting and superior/inferior tilting, and the other two are translational—medial/lateral and superior/inferior. Emerging 3-D ultrasound probe technology[21] in principle would eliminate the need for the operator to point the probe beam perfectly, as it allows full volumes to be acquired

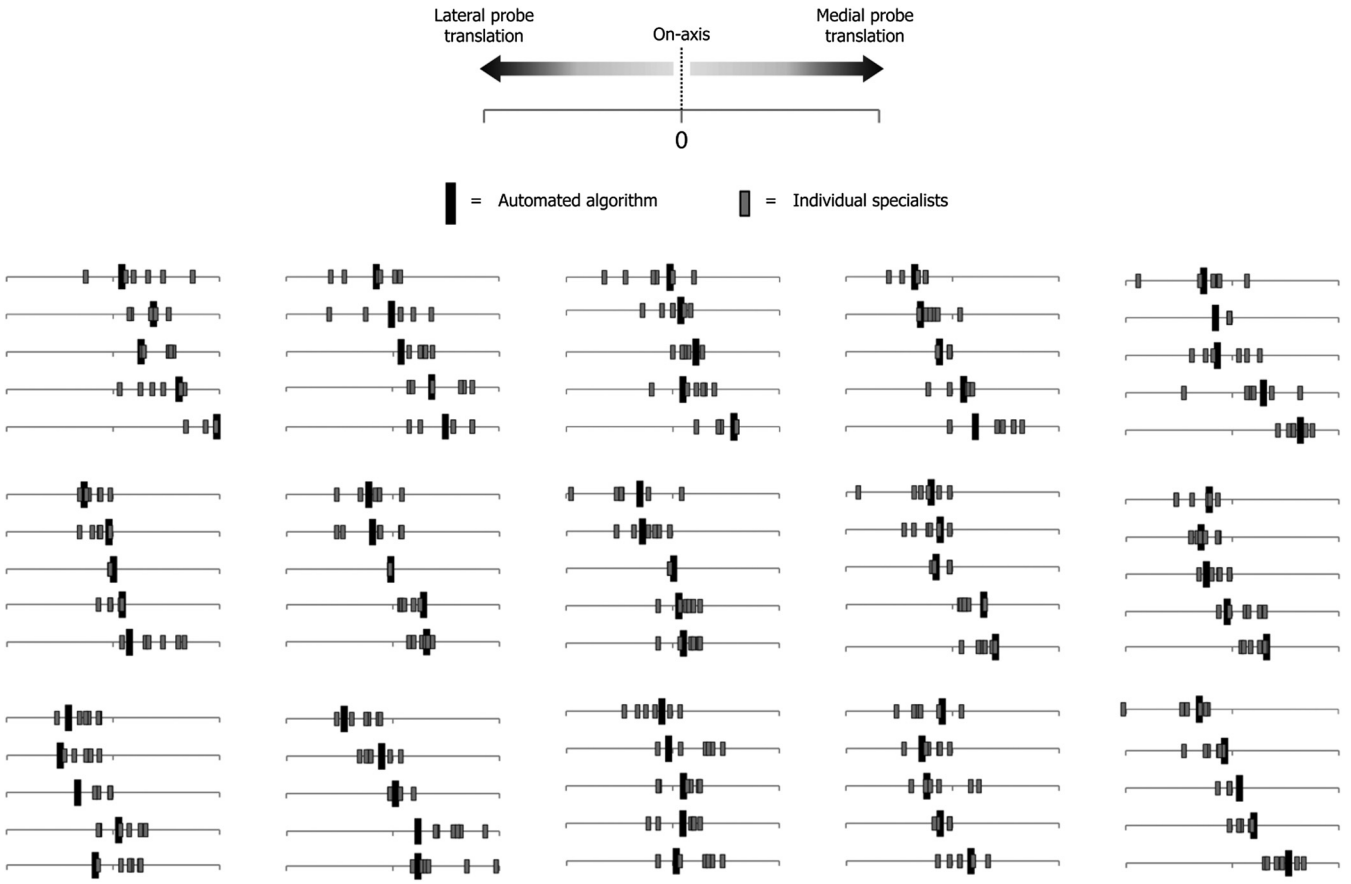

Fig. 4 Relative translation values from individual experts and the automated algorithm for all 15 subjects. Each panel of five lines represents the five images from one subject, acquired with different probe translations—arranged in order from maximum lateral translation to maximum medial translation based on consensus values). The middle of the line indicates an on-axis image, displacement to the left indicates lateral probe translation and displacement to the right indicates medial probe translation. It can be seen that in almost all cases the algorithm assessment lies well within the spectrum of expert human operator assessments. The top left subject's translations are the same as those shown in Fig. 3.

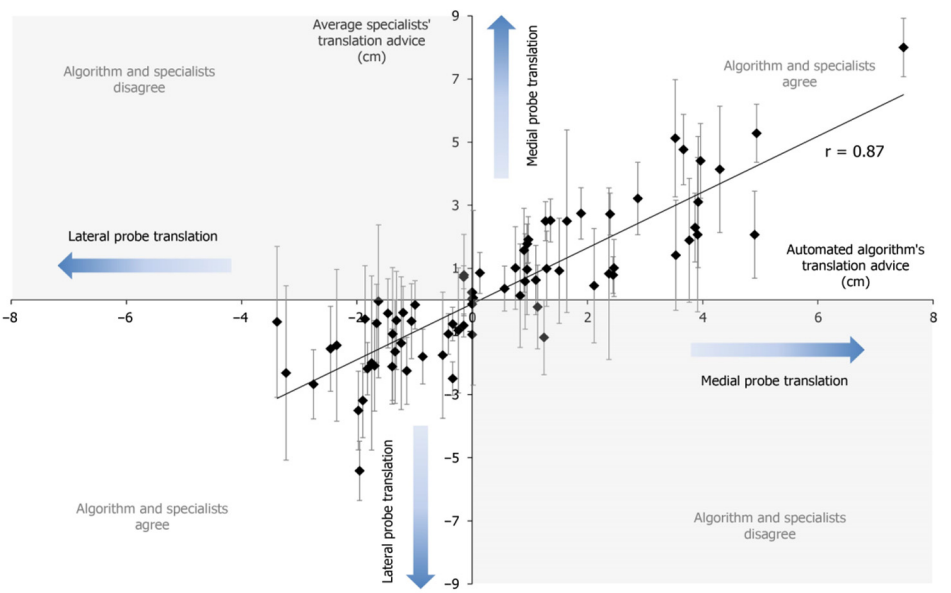

Fig. 5 Scatter plot of the average translation values of the six specialists (consensus) against the translation values from the automated algorithm. Positive displacements represent increasing medial probe translation and negative displacements represent increasing lateral probe translation. The vertical error bars show the standard deviation between the specialists.

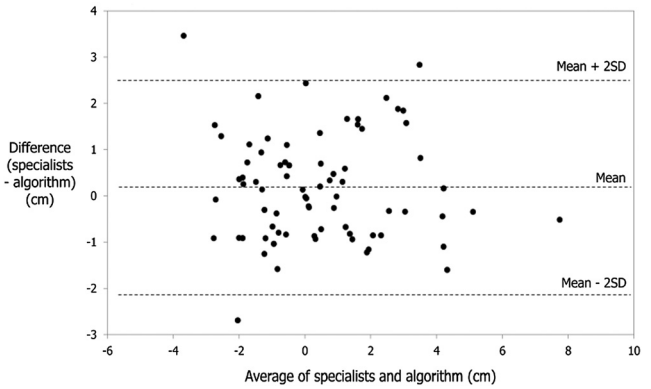

Fig. 6 Bland–Altman plot of the translation values obtained from the automated algorithm against those from the consensus of the six expert human operators.

from a single probe position. This means that the rotational degree of freedom of the probe will be automatically handled by the probe technology itself, and as long as the translational position on the chest wall is correct i.e., at the apex of the heart, all the rotational planes, i.e., the full volume will be acquired regardless of the degree of rotation of the probe. Therefore, an operator guidance system would only need to deal with the two remaining translational degrees of freedom. In this paper, we have presented an algorithm to detect medial/lateral translation, which leaves only one more degree of freedom not dealt with—superior/inferior translation. Since this plane is orthogonal to the medial/lateral plane, it is, in principle, a similar problem to the one approached in this paper; therefore, future work might use similar algorithms in order to detect motion in this plane.

4.3 *Study Limitations and Follow-Up Studies*

Due to the lack of an independent, quantitative method to measure the adequacy of orientation of an echo image, the performance of our automated algorithm had to be tested based on the assumption that the average of the specialists' values was a reasonable pragmatic ideal. Since this consensus is derived from the specialists' own judgements, it would tend to be biased to artefactually favoring the specialists, however, we have tried to eliminate this bias where possible, i.e., correlating each individual specialist's values with the consensus of the other specialists excluding that individual.

No subjects with heart disease were included in this study, therefore, the sample is not fully representative of patients. However, over half of all echocardiographic studies are normal. In addition, the algorithm is independent of any specific structures in the image and uses only overall velocities. Far less than 1% will have abnormalities so severe that the arrangement of the chambers and overall pattern of motion is different from a normal heart. Our system could in principle, in a difficult case, after multiple iterations of probe adjustment and reanalysis, automatically identify a difficult case requiring expert skills, reducing the time spent by novices when there is little chance of obtaining a standardized image.

It will also be of interest to further extend the proposed automated technique to 3-D studies. This may help to overcome foreshortening—one of the common imaging pitfalls in the apical view, where the ultrasound plane does not cut through the true apex and the assumption of the velocity vectors being aligned toward/away from the probe may be invalid. Foreshortening could potentially be detected through simultaneous application of our algorithms in the orthogonal two-chamber view.

All the automated algorithms in this study have been specifically developed for the apical four-chamber view, since it is one of the most common views used in echocardiography and it provides a substantial range of quantitative information. Further algorithm development would be required to perform a similar analysis in other views, such as the parasternal long axis view, in order to exploit the unique features in each view.

All the analysis in this study was carried out offline due to the length of time taken by the speckle tracking stage of the algorithm. In principle, all the steps shown can be carried out in real time and fed back to the operator. Future technical research will pursue the real-time execution of the automated technique by implementing the algorithms in more time-efficient programming languages and harnessing multicore computing systems for parallel processing.[18] Future clinical research will involve assessing the improvement in performance and reduction in time taken for beginners to obtain adequate images using real-time probe positioning guidance.

4.4 *Clinical Implications*

This study shows that medial and lateral translation of an ultrasound probe away from the optimum position can be reliably detected using an automated system without requiring any input from human operators. This may form part of a system where this information could be fed back to the operator and may augment current training schemes. It could potentially guide less experienced echocardiographers to obtain standardized images for accurate interpretation and analysis. This may accelerate their learning, allowing them to gain crucial early experience with less intensive and time-consuming supervision.

Such a system could also be used for quality control purposes in clinical practice as well as for research projects involving ultrasound images, as it provides an objective quantitative measure of the orientation of a four-chamber image.

The algorithm would also be a useful addition to any system making automated measurements on ultrasound images, such as selection of E and e′ measurement positions.[22] The rate of myocardial relaxation is given by the early diastolic velocity of the mitral valve annulus (e′). When combined with the early transmitral flow velocity (E), the resultant ratio (E/e′) provides an index of the left ventricular filling pressure and has both diagnostic and prognostic significance.[23] The algorithm could be used to verify that the four-chamber image is correctly orientated and, if not, guide the operator to correct the image by correcting probe position before the system makes the automated measurements.

5 Conclusion

We have presented a fully automated algorithm to quantify medial and lateral translation of an ultrasound probe for 2-D grayscale four-chamber echocardiography images. Human specialists do not perfectly agree with each other regarding medial/lateral probe positioning. The automated algorithm provides a quantitative result which accords as well with the specialists' consensus as individual specialists do.

This approach could be developed as part of a system that could be used to accelerate the learning curve for those training in echocardiography, assisting as part of an automated quality control process (for both clinical and research purposes) and

providing real-time guidance to less experienced operators to increase their chances of acquiring adequate images.

Acknowledgments

The authors are grateful to the Imperial NIHR Biomedical Research Centre scheme, the BHF Research Excellence Award Centre scheme, and the European Research Council for providing funding support for this study. D.F. and K.W. were funded by the BHF (FS/10/038). G.C. was funded by the BHF (FS/12/12/29294). M.Z. and N.D. were funded by the ERC (281524).

References

1. M. Pepi et al., "Recommendations for echocardiography use in the diagnosis and management of cardiac sources of embolism," *Eur. J. Echocardiogr.* **11**, 461–476 (2010).
2. A. N. Nowbar, G. D. Cole, and D. P. Francis, "The changing relative contribution of operator salary and hardware costs to echocardiography—a historical perspective," *Int. J. Cardiol.* **168**, 1641 (2013).
3. J. Chambers et al., "Echocardiography within the British Isles: executive summary of a British Society of Echocardiography survey," *Br. J. Cardiol.* **14**, 99–101 (2007).
4. B. A. Popescu et al., "European Association of Echocardiography recommendations for training, competence, and quality improvement in echocardiography," *Eur. J. Echocardiogr.* **10**, 893–905 (2009).
5. A. Evangelista et al., "European Association of Echocardiography recommendations for standardization of performance, digital storage and reporting of echocardiographic studies," *Eur. J. Echocardiogr.* **9**, 438–448 (2008).
6. R. M. Lang et al., "Recommendations for chamber quantification," *Eur. J. Echocardiogr.* **7**, 79–108 (2006).
7. D. P. Francis, A. J. Coats, and D. G. Gibson, "How high can a correlation coefficient be? Effects of limited reproducibility of common cardiological measures," *Int. J. Cardiol.* **69**, 185–189 (1999).
8. C. Goffinet and J.-L. Vanoverschelde, 2007, "Speckle Tracking Echocardiography. European Cardiovascular Disease," http://www.touchcardiology.com/articles/speckle-tracking-echocardiography (accessed 14 January 2014).
9. F. Orderud, H. Torp, and S. I. Rabben, "Automatic alignment of standard views in 3d echocardiograms using real-time tracking," *Proc. SPIE* **7265**, 72650D (2009).
10. L. Xiaoguang et al., "AutoMPR: Automatic detection of standard planes in 3D echocardiography," in *5th IEEE International Symposium on Biomedical Imaging: From Nano to Macro*, pp. 1279–1282, IEEE, (2008).
11. T. Karavides et al., "Database guided detection of anatomical landmark points in 3D images of the heart," in *IEEE International Symposium on Biomedical Imaging: From Nano to Macro*, pp. 1089–1092, IEEE, (2010).
12. S. R. Snare et al., "Automatic real-time view detection," in *IEEE International Ultrasonics Symposium (IUS)*, pp. 2304–2307, IEEE, (2009).
13. M. Weidenbach et al., "Augmented reality simulator for training in two-dimensional echocardiography," *Comput. Biomed. Res.* **33**(1), 11–22 (2000).
14. M. Weidenbach et al., "Computer-based training in two-dimensional echocardiography using an echocardiography simulator," *J. Am. Soc. Echocardiogr.* **18**(4), 362–366 (2005).
15. N. S. Chahal et al., "Normative reference values for the tissue Doppler imaging parameters of left ventricular function: a population-based study," *Eur. J. Echocardiogr.* **11**, 51–56 (2010).
16. L. Galiuto, G. Ignone, and A. N. DeMaria, "Contraction and relaxation velocities of the normal left ventricle using pulsed-wave tissue Doppler echocardiography," *Am. J. Cardiol.* **81**, 609–614 (1998).
17. S. A. Hojjatoleslami and J. Kittler, "Region growing: a new approach," *IEEE Trans. Image Process.* **7**, 1079–1084 (1998).
18. H. S. Wu et al., "Real-time left ventricular speckle tracking in 3D echocardiography with parallel block matching," *Int. J. Cardiol.* **164**, S13 (2013).
19. H. Blessberger and T. Binder, "Two dimensional speckle tracking echocardiography: basic principles," *Heart* **96**, 716–722 (2010).
20. J. M. Bland and D. G. Altman, "Measuring agreement in method comparison studies," *Stat. Methods Med. Res.* **8**, 135–160 (1999).
21. J. Hung et al., "3D echocardiography: a review of the current status and future directions," *J. Am. Soc. Echocardiogr.* **20**, 213–233 (2007).
22. N. M. Dhutia et al., "A new automated system to identify a consistent sampling position to make tissue Doppler and transmitral Doppler measurements of E, E′ and E/E′," *Int. J. Cardiol.* **155**, 394–349 (2012).
23. S. F. Nagueh et al., "Recommendations for the evaluation of left ventricular diastolic function by echocardiography," *J. Am. Soc. Echocardiogr.* **22**, 107–133 (2009).

Biographies of the authors are not available.